Superresolution intrinsic fluorescence imaging of chromatin utilizing native, unmodified nucleic acids for contrast

Biqin Dong[a,b,1], Luay M. Almassalha[a,1], Yolanda Stypula-Cyrus[a], Ben E. Urban[a], John E. Chandler[a], The-Quyen Nguyen[a], Cheng Sun[b], Hao F. Zhang[a,2], and Vadim Backman[a,2]

[a]Biomedical Engineering Department, Northwestern University, Evanston, IL 60208; and [b]Mechanical Engineering Department, Northwestern University, Evanston, IL 60208

Edited by Gabriel Popescu, University of Illinois at Urbana–Champaign, Urbana, IL, and accepted by Editorial Board Member John A. Rogers July 8, 2016 (received for review February 9, 2016)

Visualizing the nanoscale intracellular structures formed by nucleic acids, such as chromatin, in nonperturbed, structurally and dynamically complex cellular systems, will help expand our understanding of biological processes and open the next frontier for biological discovery. Traditional superresolution techniques to visualize subdiffractional macromolecular structures formed by nucleic acids require exogenous labels that may perturb cell function and change the very molecular processes they intend to study, especially at the extremely high label densities required for superresolution. However, despite tremendous interest and demonstrated need, label-free optical superresolution imaging of nucleotide topology under native nonperturbing conditions has never been possible. Here we investigate a photoswitching process of native nucleotides and present the demonstration of subdiffraction-resolution imaging of cellular structures using intrinsic contrast from unmodified DNA based on the principle of single-molecule photon localization microscopy (PLM). Using DNA-PLM, we achieved nanoscopic imaging of interphase nuclei and mitotic chromosomes, allowing a quantitative analysis of the DNA occupancy level and a subdiffractional analysis of the chromosomal organization. This study may pave a new way for label-free superresolution nanoscopic imaging of macromolecular structures with nucleotide topologies and could contribute to the development of new DNA-based contrast agents for superresolution imaging.

superresolution fluorescence microscopy | label-free imaging | nucleic acids | chromatin topology | chromosome

Advances in genomics and molecular biology over the past decades revolutionized our knowledge of biological systems. Despite our expanded understanding of biological interactions, there continues to be a limited understanding of these complex molecular processes in nonperturbed, structurally and dynamically complex cellular systems (1). As such, it is of critical importance to develop methods that allow direct visualization of nanoscale structures where these processes take place in their native states. Recently, superresolution fluorescence microscopy techniques, including stimulated emission depletion microscopy, structured illumination microscopy, and photon localization microscopy (PLM), such as photoactivated localization microscopy and stochastic optical reconstruction microscopy (STORM), have extended the ultimate resolving power of optical microscopy far beyond the diffraction limit (2–6), facilitating access to the organization of cells at the nanoscale by optical means. Although superresolution imaging of biological structures using labeled proteins has been well documented due to a wide range of methodologies that provide desirable labeling properties (7, 8), and despite tremendous interest and demonstrated need, there are few nanoscopic methods to image macromolecular structures formed by nucleic acids due to constraints in labeling (9–14). Likewise, the limited techniques that currently exist cannot perform label-free imaging of the native, nonperturbed macromolecular structures formed by nucleic acids.

To date, the vast majority of strategies used to image structures formed by nucleic acids require methods that label DNA-associated proteins instead of DNA itself or use small molecules that may alter the structure and function of the native structures (15, 16). For superresolution imaging, most methods take advantage of the wider availability of protein labeling, thereby using proteins commonly conjugated with nucleic acids, such as histone 2B (H2B) in eukaryotic cells (13), centromeric partition protein in bacteria (14), or centromere-associated proteins to target specific regions of chromosomes (12). This strategy has been used for indirect imaging of isolated plasmids (5) and chromatin structure in both fixed (9–12) and living cells (13, 14). However, DNA-associated proteins are not always present at the density required for superresolution imaging and, more importantly, they might not faithfully reflect the endogenous DNA topology. Therefore, development of methods to label DNA itself for superresolution imaging is highly desirable (17, 18). Recent developments including photoswitched DNA binding molecules (19–21), photoactivatable cell-permeant DNA probes (22, 23), and reversibly photoswitchable nucleosides (24) are potentially suitable for superresolution imaging of DNA topology. Single-molecule fluorescence in situ hybridization has also been combined with PLM to visualize spatial distributions of specific gene sequences with nanoscale resolution (25).

Despite remarkable progress, the exogeneous labels used in superresolution imaging of DNA topology pose several weaknesses,

Significance

Fluorescence photoswitching of native, unmodified deoxyribonucleic acid (DNA) using visible light facilitates the label-free nanoscale imaging of chromatin structures based on the principle of single-molecule photon localization microscopy (PLM). With a demonstrated sub–20-nm resolution, DNA-PLM provides an ideal technique to visualize the spatial organization of single or groups of nucleosomes and quantitatively estimate the nucleosome occupancy level of DNA in unstained chromosomes and nuclei. This study paves a way for revealing nanoscopic features of chromatin without the need for exogenous labels and could substantially expand our understanding of the structure–function relationship of chromatin.

Author contributions: B.D., L.M.A., B.E.U., T.-Q.N., C.S., H.F.Z., and V.B. designed research; B.D., L.M.A., Y.S.-C., B.E.U., and J.E.C. performed research; B.D. and L.M.A. analyzed data; and B.D., L.M.A., H.F.Z., and V.B. wrote the paper.

Conflict of interest statement: H.F.Z. and C.S. have financial interests in Opticent Health; V.B. has financial interests in NanoCytomics. Neither of these companies funded this work.

This article is a PNAS Direct Submission. G.P. is a Guest Editor invited by the Editorial Board.

Freely available online through the PNAS open access option.

[1]B.D. and L.M.A. contributed equally to this work.

[2]To whom correspondence may be addressed. Email: hfzhang@northwestern.edu or v-backman@northwestern.edu.

This article contains supporting information online at www.pnas.org/lookup/suppl/doi:10.1073/pnas.1602202113/-/DCSupplemental.

including (*i*) they require additional labeling processes; (*ii*) they perturb cell function and change the very molecular processes under investigation, especially for the high label densities necessary for superresolution (~ one label per half-resolution distance); and (*iii*) they could introduce inaccurate spatial localization caused by the physical dimension of the tagged fluorescent and linker molecules (26). The combination of these weaknesses reduces the appeal of extrinsic fluorescent contrast agents in superresolution imaging. Additionally, it has been demonstrated that natural endogenous fluorophores are potentially suitable for optical superresolution imaging, eliminating the need for extrinsic labeling (27, 28). For example, intrinsic contrast has been demonstrated using ground-state depletion (GSD) with individual molecule return, a method originally developed on regular fluorophores by the GSD action (6). So far, however, this method is not yet applicable for the majority of molecules in cells, e.g., proteins, lipids, carbohydrates, and nucleic acids. As such, despite its immense potential, the use of GSD of endogenous molecules remains questionable for applications in life science.

Significantly, we report the discovery of stochastic fluorescence switching in nucleic acids under visible light illumination. By combining the principle of PLM, we demonstrated optical superresolution imaging of native, unmodified DNA molecules, a technique we hereby call DNA-PLM. We then conducted superresolution imaging from isolated, unstained chromosomes and nuclei, revealing nanoscopic features of chromatin without the need for exogenous labels. This work paves the way for unperturbed, label-free nanoscale imaging of chromatin structure.

Results and Discussion

Fluorescence and Photoswitching of Nucleotides. Although nucleic acids have significantly weaker absorption in the visible versus UV spectrum, they exhibit low, but detectable (29), absorption due to the electron delocalization effect, in part arising from the aromatic ring (30, 31). The fluorescence emission in the visible range is significantly enhanced when the concentration reaches the level of that in interphase nuclei and metaphase chromosomes (see detailed discussion in *SI Appendix* and Figs. S1–S5). Furthermore, the long-lived fluorescence indicates the origin of observed fluorescence under visible light illumination is possibly related to intermolecular interactions, such as excimer/exciplex formation (32, 33) or charge separation/recombination (34). In this study, we chose short single-stranded polynucleotides (20-bp poly-A, G, C, and T, IDT) as model systems to investigate the fluorescence excitation and photoswitching of DNA molecules during visible excitation. As shown in Fig. 1*A*, the fluorescence spectra of the four types of polynucleotides indicate peak emissions near 580 nm under 532-nm excitation. The measured spectra were consistent with the emission spectrum of chromosome samples studied in parallel (see sample preparation in *Materials and Methods* and corresponding discussion regarding Figs. 3 and 4), which demonstrates that we are exclusively capturing fluorescence from DNA molecules.

Integration of intrinsic fluorescence with PLM requires the ability to achieve blinking single-molecule emission. Although fully mapping the electronic states in DNA molecules is a decades-old challenge (35), there is evidence indicating the existence of long-lived dark and triplet states with lifetimes as long as a few hundred milliseconds in nucleotides (36). These states can serve as primary candidates for photoinduced switching of nucleic acids by leveraging GSD with dark-state shelving and stochastic return. This phenomenon has previously been exploited for superresolution microscopy with exogenous dyes (6). The corresponding photochemical process can be described by a system of three differential equations (see detailed discussion in *SI Appendix*, Fig. S6) (37). Because the dark states have a lifetime τ much longer than that of fluorescence, the majority of molecules are "shelved" to their long-lived dark (triplet) states. Only a few molecules may return to their ground state at any given time, with the average rate of $k = 1/\tau$, where they can then be repeatedly excited to the fluorescent state. This process creates the "on" and "off" periods, or blinking, yielding the required stochastic activities for precisely locating molecules with PLM.

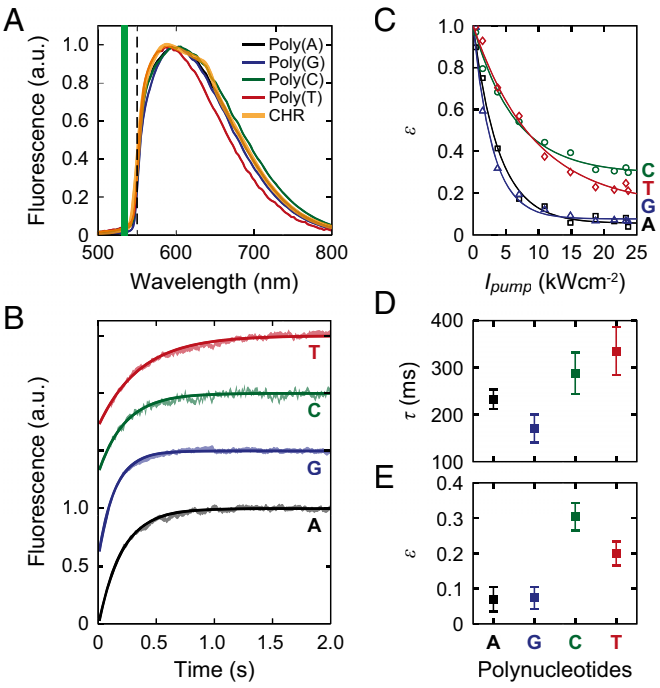

Fig. 1. (*A*) Fluorescence spectra of the polynucleotides (poly-A, G, C, and T) and isolated chromosome (CHR) sample. Fluorescence was excited by a 532-nm laser. Dashed line indicates the cutoff wavelength of long-pass dichroitic filter being used in the measurement. (*B*) Fluorescence recovery of polynucleotides after dark-state shelving (curves are shifted vertically for clarity). The recovered signal was read out (10 ms, 0.5 kWcm^{-2} of 532-nm light) after illumination for 100 ms with I_{ex} = 24 kWcm^{-2}. The characteristic recovery times were obtained by exponential fitting (colored solid lines) to the data. (*C*) Fluorescence depletion with respect to excitation intensity I_{pump}. Comparisons of (*D*) recovery lifetime between polynucleotides and (*E*) population of ground state at I_{pump} = 24 kWcm^{-2}.

The role of the long-lived dark state of polynucleotides was validated by a pump–probe method as previously discussed in ref. 6 (see details in *Materials and Methods* and *SI Appendix*, Fig. S7). As shown in Fig. 1*B*, the theory of GSD predicts that once GSD has been induced by a strong pump excitation (I_{pump} up to 24 kWcm^{-2} for 100 ms) the fluorescence induced by a weaker probe beam (I_{probe} = 0.3 kWcm^{-2}) will follow the exponential time course of the repopulation of the ground state with recovery lifetime τ. Our results show that recovery lifetimes of polynucleotides are at the hundred-millisecond level (Fig. 1*B*), which is consistent with the typical lifetime of the dark states for traditional fluorescent probes (6). Further validation of the GSD mechanism was achieved by varying I_{pump} and estimating the population of ground state ε as the ratio of fluorescence at the beginning of the recovery to the steady state. As expected, ε was inversely related to I_{pump} (Fig. 1*C*). Fig. 1 *D* and *E* further shows comparisons of the recovery lifetime and population of ground state between polynucleotides using a beam fluence of 24 kWcm^{-2}, respectively. The recovery lifetimes of the four polynucleotides are within the same order of magnitude, which facilitate PLM with stochastic photon switching of all four types of nucleotides simultaneously in DNA molecules. Notably, different polynucleotides have distinct τ and ε. Among them, nucleotides containing purines (adenine and guanine) and pyrimidines (cytosine, thymine) have similar τ and ε, respectively, likely due to the similarity of their molecular structures.

Single-Molecule Imaging of Nucleotides. To demonstrate the imaging capability of DNA-PLM, we further performed single-molecule imaging of 20-bp poly-G DNA (see detailed preparation in *Materials and Methods*). Poly-G DNA has a high dark-state shelving probability and a relatively shorter recovery lifetime compared with other investigated polynucleotides, making it ideal for demonstration. For imaging, we excited Poly-G DNA samples using a 532-nm laser with a

fluence of 3 kWcm^{-2}, which is a lower level of excitation that balances the switching rate and the rate of photobleaching (which can turn the molecules irreversibly dark). We acquired movies consisting of 5,000 frames at exposure times of 10 ms per frame. As shown in Fig. 2*A*, the averaged wide-field fluorescence image shows only diffraction-limited features. Due to the stochastic nature of photon emission and dark-state transition, the number of photons detected from a single molecule fluctuates. Fig. 2*B* shows a histogram of detected photon counts from each stochastic emission event, which shows a peak at ~250 counts and an average at ~550 counts. Based on the Nyquist criterion (38), DNA-PLM can theoretically achieve a spatial resolution of 22 nm due to the emission characteristics of polynucleotides (*SI Appendix*, Fig. S8). Next, we investigated the temporal characteristics of the stochastic fluorescence emission, as shown in Fig. 2*C*. The occurrence of stochastic emission events shows a temporal decay, which is characteristic of the exponential decay of photobleaching. Following the temporal decay stage, the stochastic emission reached an equilibrium state, with relatively stabilized stochastic emission frequency, lasting for more than 10 min before all molecules were photobleached.

Focusing on an individual molecule (as denoted by the arrow in Fig. 2*A*), we further studied the temporal properties of stochastic on–off switching from the time trace of the fluorescence signal (Fig. 2*D*). The average on-times were a few tens of milliseconds, whereas the off-times were significantly larger (ranging from several hundred milliseconds to 10 s). For the investigated molecule, the number of photons detected per fluorescence "on" event has an average of ~500 counts but can burst up to 1,900 counts. This dramatic variation may be due to the natural complexity of the electrical structure in a DNA strand. After reconstruction of all stochastic fluorescence events, we generated a PLM image by plotting their centroids (Fig. 2*E*). The centroids approximately follow a Gaussian distribution with a full width at half maximum of 18 ± 2 nm and 20 ± 2 nm in the horizontal and the vertical axis, respectively (Fig. 2*F*), suggesting DNA-PLM achieves an imaging resolution of ~20 nm. This value is consistent with our previous estimation based on the Nyquist criterion. Notably, it has been reported that long-lived states in DNA base pairs joined by hydrogen bonds decay with essentially identical kinetics as those seen in single-strained polynucleotides (39, 40). These studies suggest that double-stranded DNA molecules with double helix should have similar photophysical properties as the single-stranded polynucleotides being examined.

Validation of DNA-PLM Imaging with Labeled DNA Fibers. To validate the capability of DNA-PLM for imaging native nucleic acids structures, we used linearly deposited unlabeled single-stranded DNA fibers (a DNA purity standard, Sigma-Aldrich) as a model system (see detailed preparation in *SI Appendix*). Using 532-nm excitation, DNA-PLM produces the characteristic linear features of the DNA fibers, the origin of which is due to the nucleic acids as confirmed using two DNA specific fluorescence probes, Syto-13 and Hoechst 33342 (Thermofisher), respectively. As shown in Fig. 3 *A* and *B*, the colocalized DNA-PLM image and diffraction-limited wide-field Hoechst fluorescence image of a single DNA fiber demonstrates the capability of DNA-PLM to image DNA structures. Furthermore, conventional STORM imaging of Syto-13 stained DNA fibers performed in parallel shows the same topology captured by DNA-PLM, as shown in Fig. 3*C*. The imaging resolution of DNA-PLM is demonstrated as 20-nm resolution (Fig. 3*D*), which is comparable to images produced by conventional STORM imaging using Syto-13 dye (Fig. 3*E*).

Superresolution Imaging of Interphase Chromatin. To demonstrate the label-free imaging of DNA topology in cells, we imaged the nanoscale structure of interphase chromatin (see detailed preparation in *Materials and Methods*). Fig. 4*A* shows the wide-field fluorescence image of an isolated, unstained interphase HeLa cell nucleus. As indicated in Fig. 1*A*, the fluorescence spectrum of the sample is identical to that of polynucleotides, which demonstrated that the contrast is mostly from nucleic acids rather than proteins in the nuclei. Fig. 4 *B* and *C* shows the corresponding DNA-PLM images at different scales (also see Movie S1 for raw images and the DNA-PLM reconstruction). Clearly, the macromolecular organization of nucleic acid structures is arranged in discrete nanoclusters in interphase nuclei, which is consistent with previous reports (9, 41). We further plotted the density image by defining the density as the number of stochastic emission events per pixel (Fig. 4*D*). The density image was then converted into a binary image and segmented by grouping the emission events based on their proximity (Fig. 4*E*). The nanocluster size and the number of emission events in each nanocluster, *N*, was plotted in Fig. 3*F*. Furthermore, a quantitative analysis revealed the size distributions of nanoclusters (Fig. 4*G*) and the number of emission events per nanocluster (Fig. 4*H*), which can be useful in understanding the nanoscale organization of chromatin (41).

Investigation of chromatin organization and structure in interphase nuclei is important for gene function and activity (42). To date, superresolution studies of chromatin with extrinsic labeling are accompanied by major drawbacks such as a limited ability to reveal the spatial organization of single or groups of nucleosomes and quantitatively estimating the nucleosome occupancy level of DNA. By imaging nucleic acid molecules using intrinsic contrast, we provide a method to visualize the native structure of chromatin with nanoscale resolution. Similar to the conventional STORM in which the number of stochastic emissions could reflect the number of fluorophores, counting the number of emissions in DNA-PLM could potentially allow a quantitative estimate of the relative number

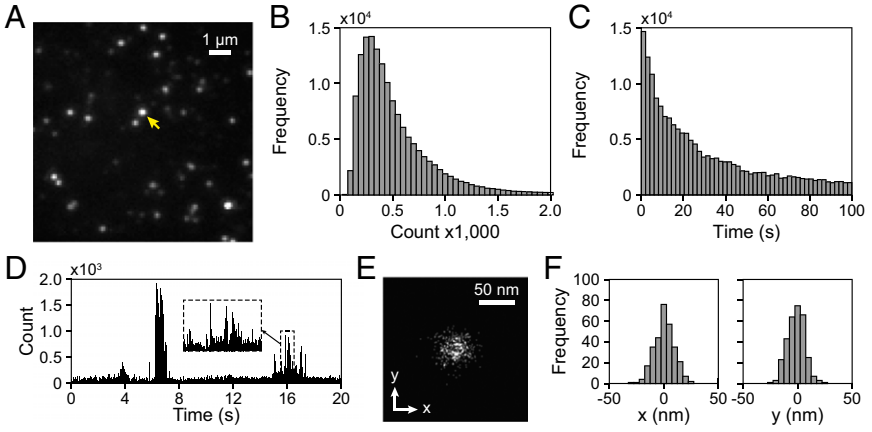

Fig. 2. (*A*) Single-molecule imaging of Poly-G DNA. (*B*) The histogram of detected photons of each switching event. (*C*) The number of events per second plotted versus time showing switching reaches a quasi-equilibrium state. (*D*) Single-molecule fluorescence time traces denoted by the arrow in *A*. (*Inset*) High zoom of the indicated region. (*E*) PLM reconstruction of the corresponding region showing stochastic emission events of a single polynucleotide. (*F*) Histograms show imaging resolutions in *x*- and *y* axis, respectively.

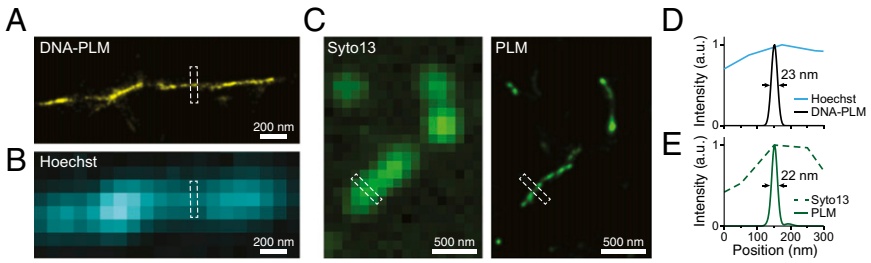

Fig. 3. (*A*) DNA-PLM image of a single DNA fiber produced using 532-nm excitation. (*B*) Colocalized diffraction-limited wide-field Hoechst 33342 fluorescence image of the same fiber as in *A* acquired using a 405-nm excitation. (*C*) Diffraction-limited wide-field fluorescence image and conventional STORM imaging of Syto-13 stained DNA fiber using a 473-nm excitation. (*D*) Comparison of transverse intensity profile between DNA-PLM and Hoechst stained DNA fiber in the region denoted by dashed boxes in *A* and *B*. (*E*) Transverse intensity profile of conventional STORM of Syto-13 stained DNA fiber, in the region denoted by dashed boxes in *C*.

of nucleotides per nanocluster. By plotting the size of the chromatin structure with respect to the number of emission events (Fig. 4*F*), a power-law scaling behavior with a scaling exponent of 0.28 ± 0.03 can be clearly observed, which is consistent with the earlier proposed chromatin organization as a fractal globule with a fractal dimension of ∼3 (43, 44). This result suggests, even at these deeply sub-diffractional length scales (20–60 nm), the topology of nucleic acids within the nucleus follows the same power-law structure as that observed at higher length scales (100–250 nm) (44, 45). At these length scales, one possible explanation is that individual genes self-assemble into discrete clusters that maximize their surface area while minimizing their volume occupancy. In this case, transcription or replication of genes could only occur on the surface of the cluster (46), as the interior would be tightly packaged with nucleic acids. Alternatively, larger clusters could be more diffuse owing to the presence of active polymerases or replicases (42). A further exploration of this topology of chromatin could only be revealed by label-free techniques such as DNA-PLM, as extrinsic labels could have nonlinear penetrance in such dense clusters.

Additionally, we observed a median cluster size of 30 nm (Fig. 4*G*), which is consistent with other studies in fixed cells showing 30-nm structures in hypotonic conditions (41, 46). To explore whether these structures form in vitro in chromatin, we performed a colocalization study on methanol fixed HeLa cells using conventional STORM immunofluorescent imaging with an Alexa Fluor 647 conjugated primary antibody targeting histone H2B and DNA-PLM (see detailed methods and results in *SI Appendix*). As shown in *SI Appendix*, Fig. S9, clusters observed by DNA-PLM frequently colocalize with the anti-histone H2B antibody. Although not every cluster colocalizes with the anti-histone H2B antibody, this could be in part the result of either steric hindrance of the antibody at these length scales or the presence of different molecular epiptopes and regulators of the cluster topology. As DNA-PLM captures the nanoscale structures formed by nucleic acids, the molecular regulators of these cluster domains could be studied in the future using novel small-molecule imaging dyes including nanobodies (47) or point accumulation for imaging in nanoscale topography (48) that could be less sensitive to steric limitations to differentially label various molecular regulators, including nucleosomes, RNA and DNA polymerases, the polycomb and cohesion complexes, and long noncoding RNA. These studies could illuminate for the first time the in vitro regulatory organization of chromatin in situ, providing both information on nucleic acid distribution and the local molecular functional states. Whereas we have demonstrated that DNA-PLM is ideal for studies of chromatin organization in fixed nuclei, as a noninvasive optical technique, DNA-PLM could potentially be suitable for nanoscopic imaging of chromatin in live cells. Through this extension, DNA-PLM would be the only technique capable of definitively answering lingering questions about the presence of the elusive 30-nm fiber in living eukaryotic cells.

Superresolution Imaging of Metaphase Chromosomes. Next, we used DNA-PLM to image the structure of isolated metaphase chromosomes (see detailed preparation in *Materials and Methods*). In particular, we focused on imaging autofluorescence of isolated X chromosomes from HeLa cells, which can be readily observed under a wide-field microscope (Fig. 5*A*), however, with diffraction-limited resolution. Using DNA-PLM, we conducted superresolution imaging of X-chromosomes, as shown in Fig. 5*B* (also see Movie S2 for raw images and the DNA-PLM reconstruction). From higher magnified images shown in Fig. 5 *C*–*E*, we can clearly see variations in nucleotide density in the thick chromatids and additional fine features which were not resolvable in the wide-field image. The segment stretched from the chromatid has a similar morphology to previously observed chromosomal fragile sites, which are specific heritable points on metaphase chromosomes that tend to form a gap, constriction, or break when cells are exposed to a perturbation during

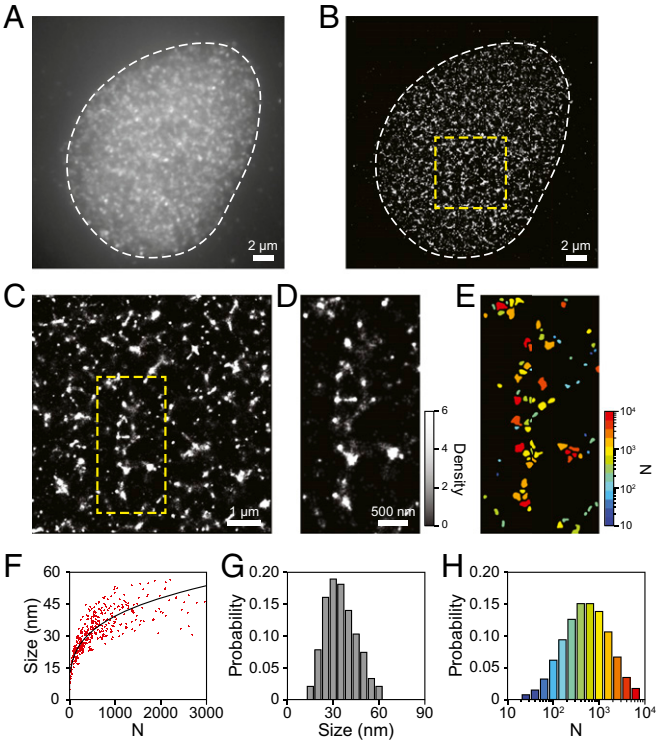

Fig. 4. (*A*) Wide-field autofluorescence image under 532-nm illumination and (*B*) DNA-PLM image of a HeLa cell nucleus. (*C*) Higher zooms of the squared region in *B*. (*D*) Density image of the indicated region in *C*, where the density is defined by the number of stochastic emission events per pixel. (*E*) The density images are converted into binary images and analyzed using a cluster identification algorithm that groups the individual localizations based on their proximity. Colors were used to denote the number of emission events in each nanocluster *N*, as indicated in *H*. (*F*) Scatter plot of cluster size and *N* indicates a power-law scaling behavior with the scaling exponents of 0.28 ± 0.03 from fitting. Statistical analysis of (*G*) the nanocluster size and (*H*) *N*.

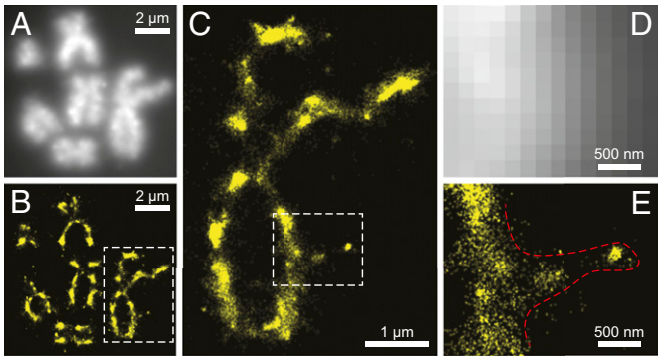

Fig. 5. (*A*) Wide-field autofluorescence image under 532-nm illumination and (*B*) DNA-PLM image of x-shaped chromosomes separated from HeLa cells. (*C*) Higher zoom of an individual chromosome shown in *B*. (*D*) Wide-field fluorescence image and (*E*) DNA-PLM image of the squared region in *C* showing additional fine features which are not resolvable in wide-field image.

DNA replication (49). Fragile sites frequently occur in the human genome and are classified as either common or rare based on their observed frequency. Observed common fragile sites are part of the normal chromosome architecture in all individuals and are of considerable interest in human diseases. In particular, common fragile sites are frequently transformed during tumorigenesis resulting in the loss of tumor suppressor genes or the formation of oncogenes (50). Likewise, rare fragile sites are seen in a small proportion of individuals, and are often associated with genetic disorders, such as fragile-X syndrome. All fragile sites are susceptible to spontaneous breakage during replication, and as such their identification and study is important to understanding diseases, including cancer.

Conclusion

Cellular autofluorescence is a widely observed phenomenon which commonly complicates immunofluorescence labeling studies. As a result, many conventional and superresolution imaging protocols use the use of reducing agents such as sodium borohydride before imaging to eliminate the intrinsic autofluorescence within the sample (7, 51). Even without the use of these reducing agents, autofluorescence can be greatly reduced simply by continuous visible light exposure of the sample before imaging (52). Consequently, the visible-light–induced autofluorescence of nucleic acids has likely been overlooked due to the broad availability of the nuclear counter stains Hoechst 33342 and DAPI, the ability to quickly eliminate the intrinsic autofluorescence within samples, and the common misperception that nucleic acids do not fluoresce within the visible range. A critical implication is that macromolecules, which are widely perceived as "dark," may be excited for superresolution imaging under different illumination conditions (27, 28, 53). The critical element in such an approach would depend on the capacity to ascertain molecular information from the intrinsic emissions of endogenous biological molecules (54).

Whereas we clearly observed the chromatin structure derived from nucleic acids, we also acknowledge that there could be some nonspecific emission events from other molecules present. The primary nucleic acid within the nucleus is DNA; however, as RNA exists within the nucleus, it may contribute to the observed blinking and the measured topology. In addition, local conjugate proteins (e.g., histones, chromatin remodeling enzymes, transcription factors, and polymerases, etc.) may also generate blinking or nonblinking background fluorescence within the nucleus. However, as shown in Fig. 1*A*, the fluorescence observed in our cellular samples is consistent with that in the ex vivo models of pure nucleic acids. This result suggests that intranuclear proteins may not be efficiently excited at the wavelengths used in imaging or the amount of them that can be excited is not significant to influence the imaging results. Thus, given the observations ex vivo, the predominant source of the signal we collected is from nucleic acids.

Finally, we note that similar switching processes can be observed under other excitations with different wavelengths (tested by 488-, 445-, and 405-nm laser illuminations). However, image quality usually suffered due to the stronger background autofluorescence and more rapid photobleaching observed at shorter wavelengths (see detailed analysis in *SI Appendix*, Fig. S10), which limited the number of stochastic emission events acquired for image reconstruction. As these different wavelengths likely excite different singlet electronic states they can, however, be used to create new switching events or to return molecules from dark states. This process is of particular use when emission events become rare due to photobleaching under prior excitation. Furthermore, specific imaging buffers, additives, or chemical methods used in chromatin fixation may vary the electronic state of DNA molecules and possibly be useful for suppressing the photobleaching or accelerating the switching of nucleotides. Follow-up studies are merited to fully understand the photophysics of DNA molecules under various conditions.

In summary, we have investigated the photoswitching process of native, unmodified DNA molecules and demonstrated the superresolution imaging capability of DNA-PLM. Using DNA-PLM we can achieve sub–20-nm resolution with unmodified DNA molecules. This technique is particularly suitable for imaging chromatin structures and may allow insight into native structures of DNA organization in cells. Understanding and controlling the mechanisms for photoinduced dark-state formation in DNA molecules is important to develop better switching, to optimize the imaging parameters, and to apply DNA-PLM to study chromatin organization in live cells. With further development, combined with temporal and spectral characterization, DNA-PLM can feasibly identify highly specific molecular "fingerprints," leading to in situ label-free sequencing of the genome. Additionally, topological and chemical alterations in highly condensed DNA strains can result in various additional photophysical interactions, as has been studied in polymer molecules, including energy transfer (55–57), ground- or excited-state aggregate formation (58, 59), and charge transfer (60). These photophysical processes can significantly modify the molecular optical properties, allowing us to further capture functional information about the chromatin nanoarchitecture.

Materials and Methods

Fluorescence Characterization. For studying the fluorescence characteristic of polynucleotides, we built an integrated optical imaging and spectroscopy system based on an inverted microscope. A 532-nm diode-pumped solid-state laser with 300-mW maximum output was passed through the microscope body (Nikon, Eclipse Ti-U) and was focused by an objective lens (Nikon, CFI Apo TIRF 100×, 1.49 N.A.). The intensity and beam size of the illumination beam fluence were controlled by a linear polarizer and a dual lens assembly. For spectral characterization, the signal was routed to a spectrometer (Princeton, SP2150i) with a 150 lines per millimeter diffraction grating and an electron multiplying charge-coupled device (EMCCD, Princeton Instruments, ProEM512B Excelon), giving a maximum 0.6-nm spectral resolution. A long-pass filter (BLP01-532R-25, Semrock) was used to reject the reflected laser beam. The primary fluorescence image was collected through a 550-nm long-pass filter before video acquisition by an EMCCD (Andor, iXon 897 Ultra) at a frame rate of 100 Hz. We determined the fraction of residual singlet-state molecules using a pump–probe mode with a constant probe (0.3 $kWcm^{-2}$) and pump pulses of varying intensity (100 ms, 1–25 $kWcm^{-2}$) for shelving the molecules into dark states. The fluorescence recovery was monitored for calculating the recovery lifetime by applying an exponential fitting.

Preparation of Polynucleotides Hydrogel and Single-Molecule Samples. The detailed methods can be found in *SI Appendix*.

Validation of DNA-PLM Imaging with Labeled DNA Fibers. The detailed preparation of single-stranded DNA sample can be found in *SI Appendix*. To validate DNA-PLM imaging of unlabeled DNA fibers, the nucleic acid origin of fibers was confirmed by staining using two DNA specific fluorescence probes, Hoechst 33342 and Syto-13. The detailed staining protocol can be found in *SI Appendix*.

Chromosome Preparation from Cultured Cells. The detailed preparation of chromosome and nuclei isolation can be found in *SI Appendix*. Isolation was performed as described previously (61) with minor modifications. Prior to imaging, 5 μL nuclease-free water (IDT) was dropped at the center of a

freshly cleaned glass slide, and the sample on the coverslip was mounted on the glass slide and sealed with dental cement.

DNA-PLM Imaging Process. Chromosome samples were placed on the microscope stage and imaged using a high-N.A. TIRF objective. Before acquiring DNA-PLM images, we used relatively weak 532-nm light (~0.3 $kWcm^{-2}$) to illuminate the sample and recorded the conventional fluorescence image. We then used a 532-nm laser with constant beam fluence of 3 $kWcm^{-2}$ to switch a substantial fraction of DNA molecules to their "off" states. We recorded images using the EMCCD camera (iXon Ultra 897, Andor). The integration time and the frame rate of image acquisition were carefully selected to provide optimal signal-to-noise ratio of the acquired image. Unless specifically noted, 10,000 frames were recorded for PLM reconstruction. For imaging of isolated chromosomes and nuclei isolated from HeLa cells, a preexposure using the same laser illumination may be required to reduce the background autofluorescence from residual organic compounds; images were then recorded in the stabilized switching stage. The optimal time duration of the preexposure process is highly sample-dependent and should be carefully adjusted according to the imaging conditions.

ACKNOWLEDGMENTS. We thank Prof. Michael R. Wasielewski for the support in photochemistry studies and Dr. Ryan M. Young, Mr. Yilei Wu, and Ms. Jenna Logsdon for assistances in spectroscopic measurements. We acknowledge the generous financial support from the National Institutes of Health (Grants T32GM008152, T32HL076139, R01EY019951, R24EY022883, and R01CA165309), the National Science Foundation (Grants DBI-1353952, CBET-1055379, CBET-1066776, EFRI-1240416, and EEC-1530734), the Chicago Biomedical Consortium Lever Award L-006 for the Chicago Center for Physical Science Oncology Innovation and Translation, and a Research Catalyst Award by Northwestern McCormick School of Engineering.

1. Ellis RJ, Minton AP (2003) Cell biology: Join the crowd. *Nature* 425(6953):27–28.
2. Hell SW, Wichmann J (1994) Breaking the diffraction resolution limit by stimulated emission: Stimulated-emission-depletion fluorescence microscopy. *Opt Lett* 19(11):780–782.
3. Gustafsson MGL (2005) Nonlinear structured-illumination microscopy: Wide-field fluorescence imaging with theoretically unlimited resolution. *Proc Natl Acad Sci USA* 102(37):13081–13086.
4. Betzig E, et al. (2006) Imaging intracellular fluorescent proteins at nanometer resolution. *Science* 313(5793):1642–1645.
5. Rust MJ, Bates M, Zhuang X (2006) Sub-diffraction-limit imaging by stochastic optical reconstruction microscopy (STORM). *Nat Methods* 3(10):793–795.
6. Fölling J, et al. (2008) Fluorescence nanoscopy by ground-state depletion and single-molecule return. *Nat Methods* 5(11):943–945.
7. Dempsey GT, Vaughan JC, Chen KH, Bates M, Zhuang X (2011) Evaluation of fluorophores for optimal performance in localization-based super-resolution imaging. *Nat Methods* 8(12):1027–1036.
8. Flors C (2011) DNA and chromatin imaging with super-resolution fluorescence microscopy based on single-molecule localization. *Biopolymers* 95(5):290–297.
9. Matsuda A, et al. (2010) Condensed mitotic chromosome structure at nanometer resolution using PALM and EGFP- histones. *PLoS One* 5(9):e12768.
10. Gunkel M, et al. (2009) Dual color localization microscopy of cellular nanostructures. *Biotechnol J* 4(6):927–938.
11. Bohn M, et al. (2010) Localization microscopy reveals expression-dependent parameters of chromatin nanostructure. *Biophys J* 99(5):1358–1367.
12. Ribeiro SA, et al. (2010) A super-resolution map of the vertebrate kinetochore. *Proc Natl Acad Sci USA* 107(23):10484–10489.
13. Wombacher R, et al. (2010) Live-cell super-resolution imaging with trimethoprim conjugates. *Nat Methods* 7(9):717–719.
14. Ptacin JL, et al. (2010) A spindle-like apparatus guides bacterial chromosome segregation. *Nat Cell Biol* 12(8):791–798.
15. Beerman TA, et al. (1992) Effects of analogs of the DNA minor groove binder Hoechst 33258 on topoisomerase II and I mediated activities. *Biochim Biophys Acta* 1131(1):53–61.
16. Almassalha LM, et al. (2016) *Live cell partial wave spectroscopic microscopy: Label-free imaging of the native, living cellular nanoarchitecture*, preprint.
17. Jungmann R, et al. (2010) Single-molecule kinetics and super-resolution microscopy by fluorescence imaging of transient binding on DNA origami. *Nano Lett* 10(11):4756–4761.
18. Armitage BA (2005) Cyanine dye-DNA interactions: Intercalation, groove binding, and aggregation. *Top Curr Chem* 253:55–76.
19. Andersson J, Li S, Lincoln P, Andréasson J (2008) Photoswitched DNA-binding of a photochromic spiropyran. *J Am Chem Soc* 130(36):11836–11837.
20. Di Pietro ML, et al. (2010) Photochemically driven intercalation of small molecules into DNA by in situ irradiation. *Chem Commun (Camb)* 46(28):5169–5171.
21. Zessin PJM, Finan K, Heilemann M (2012) Super-resolution fluorescence imaging of chromosomal DNA. *J Struct Biol* 177(2):344–348.
22. Feng S, Kim YK, Yang S, Chang YT (2010) Discovery of a green DNA probe for live-cell imaging. *Chem Commun (Camb)* 46(3):436–438.
23. Erve A, et al. (2006) BENA435, a new cell-permeant photoactivated green fluorescent DNA probe. *Nucleic Acids Res* 34(5):e43.
24. Singer M, Jäschke A (2010) Reversibly photoswitchable nucleosides: Synthesis and photochromic properties of diarylethene-functionalized 7-deazaadenosine derivatives. *J Am Chem Soc* 132(24):8372–8377.
25. Weiland Y, Lemmer P, Cremer C (2011) Combining FISH with localisation microscopy: Super-resolution imaging of nuclear genome nanostructures. *Chromosome Res* 19(1):5–23.
26. Deschout H, et al. (2014) Precisely and accurately localizing single emitters in fluorescence microscopy. *Nat Methods* 11(3):253–266.
27. Bierwagen J, et al. (2010) Far-field autofluorescence nanoscopy. *Nano Lett* 10(10): 4249–4252.
28. Kaufmann R, Müller P, Hausmann M, Cremer C (2011) Imaging label-free intracellular structures by localisation microscopy. *Micron* 42(4):348–352.
29. Prahl S (2012) PhotochemCAD spectra: compounds by class (Oregon Medical Laser Center, Portland, OR). Available at omlc.org/spectra/PhotochemCAD/class.html. Accessed October 15, 2015.
30. Callis PR (1983) Electronic states and luminescence of nucleic-acid systems. *Annu Rev Phys Chem* 34:329–357.
31. Voet D, Gratzer WB, Cox RA, Doty P (1963) Absorption spectra of nucleotides, polynucleotides, and nucleic acids in the far ultraviolet. *Biopolymers* 1(3):193–208.
32. Anders A (1981) DNA fluorescence at room-temperature excited by means of a dye-laser. *Chem Phys Lett* 81(2):270–272.
33. Plessow R, Brockhinke A, Eimer W, Kohse-Hoinghaus K (2000) Intrinsic time- and wavelength-resolved fluorescence of oligonucleotides: A systematic investigation using a novel picosecond laser approach. *J Phys Chem B* 104(15):3695–3704.
34. Vayá I, Gustavsson T, Miannay FA, Douki T, Markovitsi D (2010) Fluorescence of natural DNA: From the femtosecond to the nanosecond time scales. *J Am Chem Soc* 132(34):11834–11835.
35. Middleton CT, et al. (2009) DNA excited-state dynamics: From single bases to the double helix. *Annu Rev Phys Chem* 60:217–239.
36. Crespo-Hernández CE, Cohen B, Hare PM, Kohler B (2004) Ultrafast excited-state dynamics in nucleic acids. *Chem Rev* 104(4):1977–2019.
37. Hell SW, Kroug M (1995) Ground-state-depletion fluorescence microscopy - a concept for breaking the diffraction resolution limit. *Appl Phys B* 60(5):495–497.
38. Jones SA, Shim SH, He J, Zhuang X (2011) Fast, three-dimensional super-resolution imaging of live cells. *Nat Methods* 8(6):499–508.
39. Crespo-Hernández CE, Cohen B, Kohler B (2005) Base stacking controls excited-state dynamics in A.T DNA. *Nature* 436(7054):1141–1144.
40. Buchvarov I, Wang Q, Raytchev M, Trifonov A, Fiebig T (2007) Electronic energy delocalization and dissipation in single- and double-stranded DNA. *Proc Natl Acad Sci USA* 104(12):4794–4797.
41. Ricci MA, Manzo C, García-Parajo MF, Lakadamyali M, Cosma MP (2015) Chromatin fibers are formed by heterogeneous groups of nucleosomes in vivo. *Cell* 160(6):1145–1158.
42. Papantonis A, Cook PR (2010) Genome architecture and the role of transcription. *Curr Opin Cell Biol* 22(3):271–276.
43. Lieberman-Aiden E, et al. (2009) Comprehensive mapping of long-range interactions reveals folding principles of the human genome. *Science* 326(5950):289–293.
44. Mirny LA (2011) The fractal globule as a model of chromatin architecture in the cell. *Chromosome Res* 19(1):37–51.
45. Boettiger AN, et al. (2016) Super-resolution imaging reveals distinct chromatin folding for different epigenetic states. *Nature* 529(7586):418–422.
46. Maeshima K, Hihara S, Eltsov M (2010) Chromatin structure: Does the 30-nm fibre exist in vivo? *Curr Opin Cell Biol* 22(3):291–297.
47. Pleiner T, et al. (2015) Nanobodies: Site-specific labeling for super-resolution imaging, rapid epitope-mapping and native protein complex isolation. *eLife* 4:e11349.
48. Legant WR, et al. (2016) High-density three-dimensional localization microscopy across large volumes. *Nat Methods* 13(4):359–365.
49. Schwartz M, Zlotorynski E, Kerem B (2006) The molecular basis of common and rare fragile sites. *Cancer Lett* 232(1):13–26.
50. Fungtammasan A, Walsh E, Chiaromonte F, Eckert KA, Makova KD (2012) A genome-wide analysis of common fragile sites: What features determine chromosomal instability in the human genome? *Genome Res* 22(6):993–1005.
51. Schnell SA, Staines WA, Wessendorf MW (1999) Reduction of lipofuscin-like autofluorescence in fluorescently labeled tissue. *J Histochem Cytochem* 47(6):719–730.
52. Neumann M, Gabel D (2002) Simple method for reduction of autofluorescence in fluorescence microscopy. *J Histochem Cytochem* 50(3):437–439.
53. Urban BE, et al. (2016) Subsurface super-resolution imaging of unstained polymer nanostructures. *Sci Rep* 6:28156.
54. Dong B, et al. (2016) Super-resolution spectroscopic microscopy via photon localization. *Nat Commun* 7:12290.
55. Bout DAV, et al. (1997) Discrete intensity jumps and intramolecular electronic energy transfer in the spectroscopy of single conjugated polymer molecules. *Science* 277(5329):1074–1077.
56. Yu J, Hu D, Barbara PF (2000) Unmasking electronic energy transfer of conjugated polymers by suppression of O(2) quenching. *Science* 289(5483):1327–1330.
57. Brédas J-L, Beljonne D, Coropceanu V, Cornil J (2004) Charge-transfer and energy-transfer processes in π-conjugated oligomers and polymers: A molecular picture. *Chem Rev* 104(11): 4971–5004.
58. Romaner L, et al. (2003) The origin of green emission in polyfluorene-based conjugated polymers: On-chain defect fluorescence. *Adv Funct Mater* 13(8):597–601.
59. Nguyen T-Q, Doan V, Schwartz BJ (1999) Conjugated polymer aggregates in solution: Control of interchain interactions. *J Chem Phys* 110(8):4068–4078.
60. Noone KM, et al. (2011) Photoinduced charge transfer and polaron dynamics in polymer and hybrid photovoltaic thin films: Organic vs inorganic acceptors. *J Phys Chem C* 115(49):24403–24410.
61. Howe B, Umrigar A, Tsien F (2014) Chromosome preparation from cultured cells. *J Vis Exp* 83:e50203.